$Al_{0.52}In_{0.48}P$ ^{55}Fe x-ray-photovoltaic battery

2016 J. Phys. D: Appl. Phys. 49 355601

(http://iopscience.iop.org/0022-3727/49/35/355601)

OPEN ACCESS
IOP Publishing
Journal of Physics D: Applied Physics
J. Phys. D: Appl. Phys. **49** (2016) 355601 (7pp)
doi:10.1088/0022-3727/49/35/355601

$Al_{0.52}In_{0.48}P$ ^{55}Fe x-ray-photovoltaic battery

S Butera[1,3], G Lioliou[1], A B Krysa[2] and A M Barnett[1]

[1] Semiconductor Materials and Device Laboratory, School of Engineering and Informatics, University of Sussex, Brighton, BN1 9QT, UK
[2] EPSRC National Centre for III–V Technologies, University of Sheffield, Mappin Street, Sheffield, S1 3JD, UK

E-mail: S.Butera@sussex.ac.uk

Received 4 April 2016, revised 26 May 2016
Accepted for publication 28 June 2016
Published 1 August 2016

Abstract

An $Al_{0.52}In_{0.48}P$ ^{55}Fe radioisotope microbattery is demonstrated over the temperature range −20 °C to 160 °C. $Al_{0.52}In_{0.48}P$ p^+-i-n^+ mesa structures were used to collect the photons from a 238 MBq ^{55}Fe radioisotope x-ray source. The effects of temperature on the key microbattery parameters were studied. Increasing the temperature, the saturation current increased; whilst the open circuit voltage, the maximum power and the conversion efficiency decreased. An open circuit voltage of 0.97 V and a conversion efficiency of 22% were measured in a single p^+-i-n^+ mesa structure at −20 °C. The highest total microbattery maximum output power using two mesa structures was 1.2 pW at −20 °C.

Keywords: AlInP, x-ray, photovoltaic, battery, semiconductors

(Some figures may appear in colour only in the online journal)

1. Introduction

The ability to supply small amounts of power over long periods of time is becoming increasingly important in many applications including microelectromechanical system technologies [1], biomedical [2] and aerospace applications [3]. Nuclear microbatteries, converting nuclear energy to electrical energy [4], could be used in these scenarios. In a nuclear microbattery, radioactive sources are coupled to conversion materials: the conversion material absorbs the high-energy particles emitted by the radioactive source generating electrical current. In contrast with traditional power supplies, such as chemical batteries, nuclear microbatteries offer important characteristics such as high energy density, stability, and long life. Wide bandgap semiconductors (e.g. diamond, SiC, GaAs) can be used as conversion materials in this type of system. Because of their wide bandgap, they present higher efficiency than alternative narrower bandgap materials such as silicon; this is due to the linear dependence of the conversion efficiency with bandgap [5]. Moreover, they could be advantageous in all the applications where the environment temperature can vary significantly during use as they are able to work over a broad range of temperature offering good electron mobility and low leakage current [6–9]. Recently, different alpha, beta and x-ray microbatteries have been proven [5, 10–16]. Alpha and beta emitters have received research interest because they have higher specific energy per Curie compared to x-ray emitters (e.g. 0.017 $\mu W \cdot g\,(Ci \cdot cm^2)^{-1}$ for ^{55}Fe and 0.3 $\mu W \cdot g\,(Ci \cdot cm^2)^{-1}$ for the beta emitter ^{147}Pm [4]), thus offering a higher output power. The advantages of alpha and beta microbatteries in future NASA mission are reported by Landis *et al* [14]; a critical issue for alphavoltaic converters is radiation damage by the particles, this is minimised in phosphorus-containing III–V compounds such as InGaP, ^{210}Po-InGaP alpha-voltaic microbattery have been successfully proven and analysed in [14]. Bormashov *et al* [10] demonstrated a ^{63}Ni-diamond beta-voltaic microbattery and a ^{238}Pu-diamond alpha-voltaic microbattery with conversion efficiencies as high as 0.6% and 3.6%, respectively, at room temperature. Chandrashekhar *et al* proved a ^{63}Ni-SiC microbattery with at least 6% efficiency [5], whilst Eiting *et al* a ^{33}P-SiC microbattery with 4.5% efficiency [17]. Cheng *et al* [15] reported a high open circuit voltage (1.64 V) ^{63}Ni-GaN beta-voltaic microbattery with conversion efficiency of 0.98%, at room temperature. Betavoltaic cells were also proven by Sharma *et al* [16] using P3HT

[3] Author to whom correspondence should be addressed.

semiconductive conjugated polymer; conversion efficiency as high as 0.78 was achieved at an e-beam energy of 10 keV. X-ray emitters have been also studied with particular attention; the electron capture x-ray emitter ^{55}Fe has the advantage of reduced device damage risk due to the low energy photons emitted, can be easily shielded providing safer working conditions, and is readily commercially available. Butera *et al* [13] reported a GaAs ^{55}Fe radioisotope x-ray microbattery working over the temperature range −20 °C to 70 °C, with a maximum output power of 1 pW (corresponding to 0.4 μW/Ci) and conversion efficiency of 9% at −20 °C. A III–V wide bandgap ternary compound that could be very useful as the conversion layer in a nuclear microbattery is $Al_{0.52}In_{0.48}P$. $Al_{0.52}In_{0.48}P$ has an indirect bandgap of ~2.3 eV [18, 19], and it is lattice matched with GaAs. $Al_{0.52}In_{0.48}P$ is widely used in semiconductor optoelectronics and the crystalline quality of the lattice matched $Al_{0.52}In_{0.48}P$ can be very high in comparison to III–V nitrides, IV and II–VI compounds of a similar bandgap. The doping in $Al_{0.52}In_{0.48}P$ is also easier to control than in some II–VI semiconductors. In this paper for the first time a $Al_{0.52}In_{0.48}P$ ^{55}Fe radioisotope microbattery is demonstrated. A p^+-i-n^+ $Al_{0.52}In_{0.48}P$ structure was used to collect the photons from a 238 MBq ^{55}Fe radioisotope x-ray source; the changes in the key microbattery parameters were studied over the temperature range −20 °C to 160 °C.

2. Device structure

Two 400 μm diameter unpassivated p^+-i-n^+ $Al_{0.52}In_{0.48}P$ mesa photodiodes (D1 and D2), located on the same chip, were illuminated by a 238 MBq ^{55}Fe radioisotope x-ray source (Mn $K\alpha = 5.9$ keV, Mn $K\beta = 6.49$ keV). The x-ray emitter was 5 mm away from top surface of the detectors. The $Al_{0.52}In_{0.48}P$ epilayer of the devices was grown by metalorganic vapour phase epitaxy (MOVPE) on a commercial (1 0 0) n-GaAs: Si substrate with a misorientation of 10 degrees towards <1 1 1> A to suppress the CuPt-like ordered phase. The doping concentrations of the $Al_{0.52}In_{0.48}P$ p^+ and n^+ layers were 5×10^{17} cm^{-3} and 2×10^{18} cm^{-3}, respectively. The layers' thicknesses were 0.2 μm for the p^+-region, 2 μm for the i-region and 0.1 μm for the n^+-region. After growth, the wafer was processed to form mesa structures using 1:1:1 H_3PO_4:H_2O_2:H_2O solution followed by 10 s in 1:8:80 H_2SO_4: H_2O_2: H_2O solution. An Ohmic rear contact consisting of 20 nm of InGe and 200 nm of Au was evaporated onto the rear of the substrate and an Ohmic top contact consisting of 20 nm of Ti and 200 nm of Au was evaporated on the p-side of the mesa device. The top Ohmic contact covered 33% of the surface of each 400 μm diameter photodiode. The device layers, their relative thicknesses and materials are summarised in table 1. Figure 1 shows a schematic cross sectional view of the $Al_{0.52}In_{0.48}P$ mesa structure.

The x-ray quantum efficiency (QE) of a semiconductor detector is defined as the percentage of x-ray photons absorbed by the photodetector. Using the Beer–Lambert law and assuming complete charge collection in the active p- and i-layers, x-ray quantum efficiencies (QE) of 20% and 16% were calculated for the device for 5.9 keV and 6.49 keV photons, respectively, considering the GaAs dead region. The QE values were calculated, according equation (1), taking into account that 33% of the device surface was covered by the top metal contact.

Table 1. Layer details of the $Al_{0.52}In_{0.48}P$ photodiode.

Layer	Material	Thickness (μm)	Dopant	Dopant type	Doping density (cm^{-3})
1	Ti	0.02			
2	Au	0.2			
3	GaAs	0.01	Zn	p^+	1×10^{19}
4	$Al_{0.52}In_{0.48}P$	0.2	Zn	p^+	5×10^{17}
5	$Al_{0.52}In_{0.48}P$	2	Undoped		
6	$Al_{0.52}In_{0.48}P$	0.1	Si	n^+	2×10^{18}
7	Substrate n^+ GaAs				
8	Au	0.2			
9	InGe	0.02			

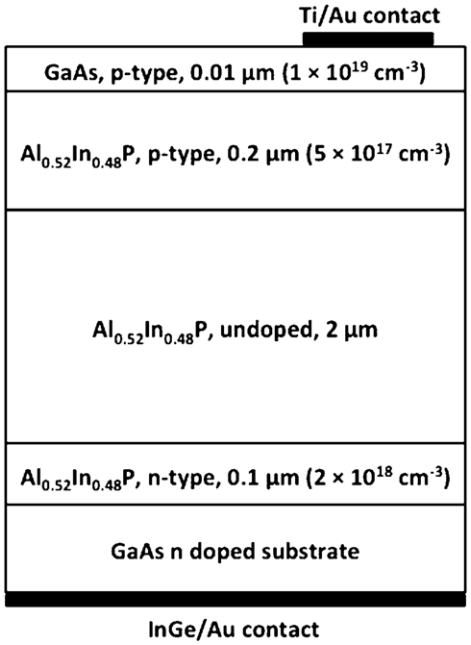

Figure 1. Schematic cross sectional view of the $Al_{0.52}In_{0.48}P$ mesa structure.

$$QE = [0.67 + 0.33\exp(-\mu_{Ti}d_{Ti})\exp(-\mu_{Au}d_{Au})]$$
$$\exp(-\mu_{GaAs}d_{GaAs})(1 - \exp(-\mu_{AlInP}d_{AlInP})) \quad (1)$$

where μ_{Ti} and d_{Ti} are the linear attenuation coefficient and thickness of Ti, μ_{Au} and d_{Au} are the linear attenuation coefficient and thickness of Au, μ_{GaAs} and d_{GaAs} are the linear attenuation coefficient and thickness of GaAs, μ_{AlInP} and d_{AlInP} are the linear attenuation coefficient and the thickness of the active region of $Al_{0.52}In_{0.48}P$. The $Al_{0.52}In_{0.48}P$ attenuation coefficients, used to calculate the quantum efficiency at 5.9 keV and 6.49 keV, were estimated to be 0.1109 μm^{-1} and 0.0856 μm^{-1} [20, 21]; whilst the GaAs, Ti and Au attenuation coefficients at 5.9 keV and 6.49 keV were taken after [20, 22].

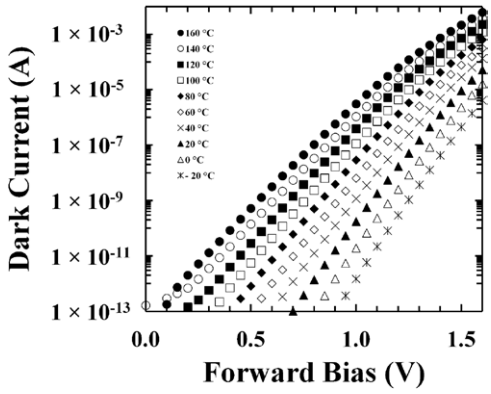

Figure 2. Dark current as a function of applied forward bias for D1. The temperatures studied were 160 °C (filled circles), 140 °C (empty circles), 120 °C (filled squares), 100 °C (empty squares), 80 °C (filled rhombuses), 60 °C (empty rhombuses), 40 °C (crosses), 20 °C (filled triangles), 0 °C (empty triangles) and −20 °C (stars).

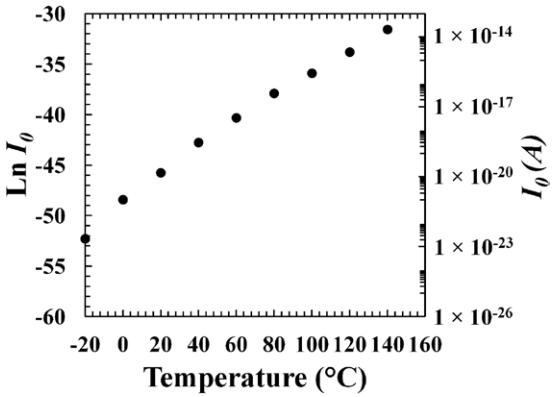

Figure 3. The logarithm of the saturation current (left *y*-axis) and the saturation current (right *y*-axis) as a function of temperature in D1.

3. Results and discussion

The $Al_{0.52}In_{0.48}P$ ^{55}Fe radioisotope microbattery was investigated over the temperature range −20 °C to 160 °C using a TAS Micro MT climatic cabinet with a dry nitrogen atmosphere (relative humidity <5%). At each analysed temperature, dark and illuminated current characteristics of each $Al_{0.52}In_{0.48}P$ p^+-i-n^+ photodiode (D1 and D2) were measured as functions of applied bias. Forward bias measurements from 0 V to 1.6 V were made in 0.01 V increments using a Keithley 6487 picoammeter/voltage source. The uncertainty associated with the current readings was 0.3% of their values plus 400 fA, while the uncertainty associated with the applied biases was 0.1% of their values plus 1 mV [23]. Figure 2 shows typical dark current characteristics as a function of forward bias at different temperatures.

In both the analysed $Al_{0.52}In_{0.48}P$ photodiodes, the dark currents increased as a function of applied bias, this was due to the greater electric fields across the i-region in each $Al_{0.52}In_{0.48}P$ structure. At high temperatures, the dark currents through the devices also increased due to the higher thermal energy available. At each temperature, a linear least square fit on the dark current data as a function of applied bias was used to extrapolate the saturation current (I_0) in both detectors

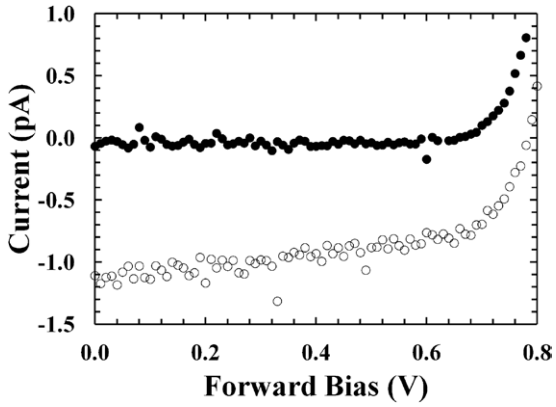

Figure 4. Dark (filled circles) and illuminated (empty circles) current characteristics as functions of applied bias for D1 at 20 °C.

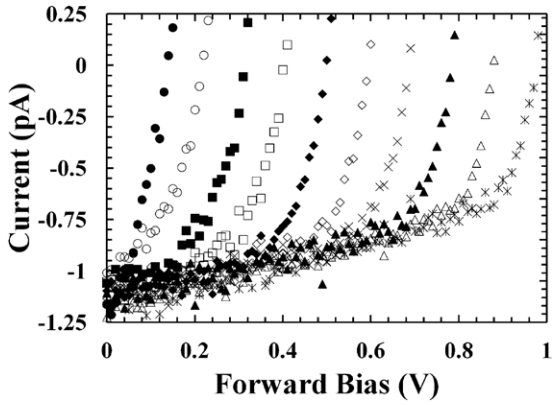

Figure 5. Current as a function of applied forward bias for D1 under illumination of the ^{55}Fe x-ray radioactive source. The temperatures studied were 160 °C (filled circles), 140 °C (empty circles), 120 °C (filled squares), 100 °C (empty squares), 80 °C (filled rhombuses), 60 °C (empty rhombuses), 40 °C (crosses), 20 °C (filled triangles), 0 °C (empty triangles) and −20 °C (stars).

[11, 13]. Figure 3 shows the measured relationship between the logarithm of the saturation current and the temperature for D1. Similar results were obtained for D2.

The magnitude of the observed natural logarithm of the saturation current decreased at higher temperatures. From −20 °C to 160 °C this decrease was 22.19 ± 0.13 for D1 and 22.18 ± 0.10 for D2. These values were in remarkable agreement with the expected decrease 22.27. The expected decrease was calculated as per [13], with using the assumption that the temperature dependence of the saturation current was proportional to $\exp(-E_g/2kT)$ [24].

Figure 4 shows typical dark and illuminated current characteristics as functions of applied bias for D1 at 20 °C. Similar results were obtained for D2 at the same temperature.

The dark current increased exponentially as a function of applied bias ($\propto \exp\{qV/nkT\}$ where n is the ideality factor, k is the Boltzmann constant and T is the temperature) [6]. For both diodes, a linear least squares fit of the data showed that the natural logarithm of the dark current was linearly dependent on the applied forward bias. The gradients determined by the linear least squares fits were (22.23 ± 0.10) AV^{-1} and (22.36 ± 0.07) AV^{-1} for D1 and D2, respectively. Ideality factors as high as 1.779 ± 0.008 and 1.769 ± 0.006

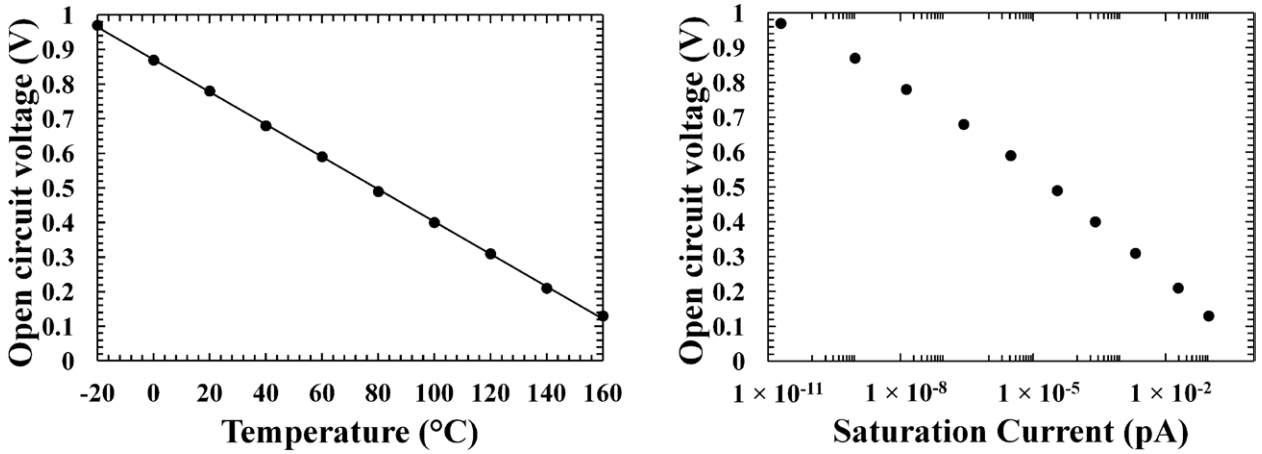

Figure 6. (a) Open circuit voltage as a function of temperature for a single cell of the $Al_{0.52}In_{0.48}P$ ^{55}Fe radioisotope microbattery; in particular, results from D1 under illumination of the ^{55}Fe x-ray source are shown. (b) Open circuit voltage as a function of saturation current for D1.

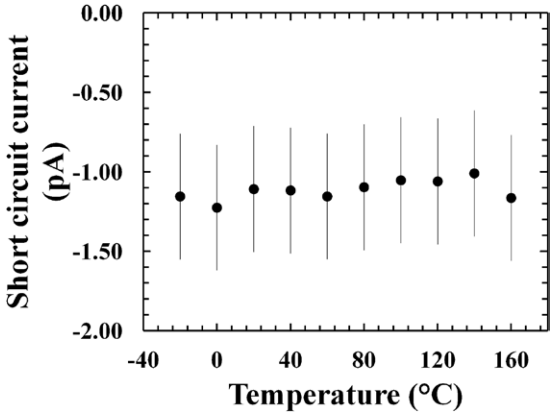

Figure 7. Short circuit current as a function of temperature for a single cell of the $Al_{0.52}In_{0.48}P$ ^{55}Fe radioisotope microbattery; in particular, results from D1 under illumination of the ^{55}Fe x-ray source are shown.

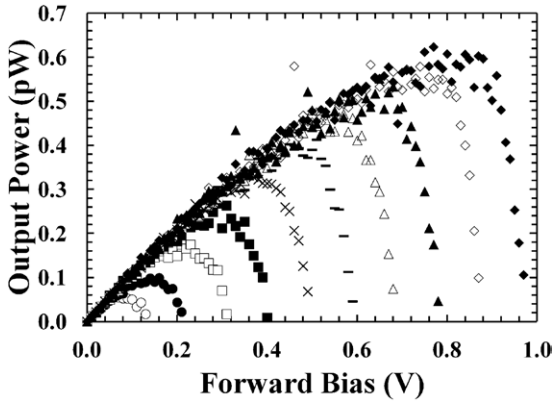

Figure 8. Output power as a function of applied forward bias for D1 at different temperatures. The temperatures studied were 160 °C (filled rhombuses), 140 °C (empty rhombuses), 120 °C (filled triangles), 100 °C (empty triangles), 80 °C (dashes), 60 °C (crosses), 40 °C (filled squares), 20 °C (empty squares), 0 °C (filled circles) and −20 °C (empty circles).

were estimated for D1 and D2, respectively. These ideality factors (close to 2) indicated that generation-recombination currents were dominant over the diffusion currents in the devices. Under the illumination of the ^{55}Fe radioisotope x-ray source, the measured current through the devices (empty circles in figure 4) increased as photocurrent is added to the dark current. X-ray photons were absorbed by the detector creating electron–hole pairs as a consequence of the photoelectric effect. Electrons and holes in the device depletion region were, thus, swept to the p^+-type and n^+-type regions, respectively, generating in the device the observed photocurrent. In figure 4, the decrease in photocurrent, observed between 0 V and 0.8 V, was smaller than its uncertainty (0.08 ± 0.8) pA.

Under the illumination of the ^{55}Fe radioisotope x-ray source, the currents through both devices were measured over the temperature range −20 °C to 160 °C. Figure 5 shows typical current characteristics as a function of forward bias at different temperatures for D1. Similar results were obtained for D2.

At increased temperature, the softness in the knee of the measured current as a function of applied forward bias decreased in both photodiodes. The experimental values of the open circuit voltage (V_{OC}) were obtained as the interception point of the curves in figure 5 on the horizontal axis. Figure 6(a) shows the V_{OC} as a function of temperature for D1; a similar behaviour was found also for D2. At increased temperature, the open circuit voltage decreased because of its dependent on the saturation current (I_0) [6]. V_{OC} increased logarithmically with decreasing I_0, according equation (2):

$$V_{OC} \sim \frac{kT}{q} \ln\left(\frac{I_{ph}}{I_0}\right) \tag{2}$$

where k is the Boltzmann constant, T is the temperature, I_{ph} is the photocurrent through the device and I_0 the saturation current [6]. Figure 6(b) shows the experimental dependence found between the open circuit and the saturation current for D1.

The open circuit voltage (V_{OC}) was measured to decrease linearly with temperature in both the analysed detectors. Over the range of temperature −20 °C to 160 °C, $V_{OC} = -AT + B$: $A = (0.004\,60 \pm 0.000\,03)$ V °C^{-1}, $B = (0.871 \pm 0.002)$ V for D1 and $A = (0.004\,60 \pm 0.000\,02)$ V °C^{-1}, $B = (0.866 \pm 0.002)$ V

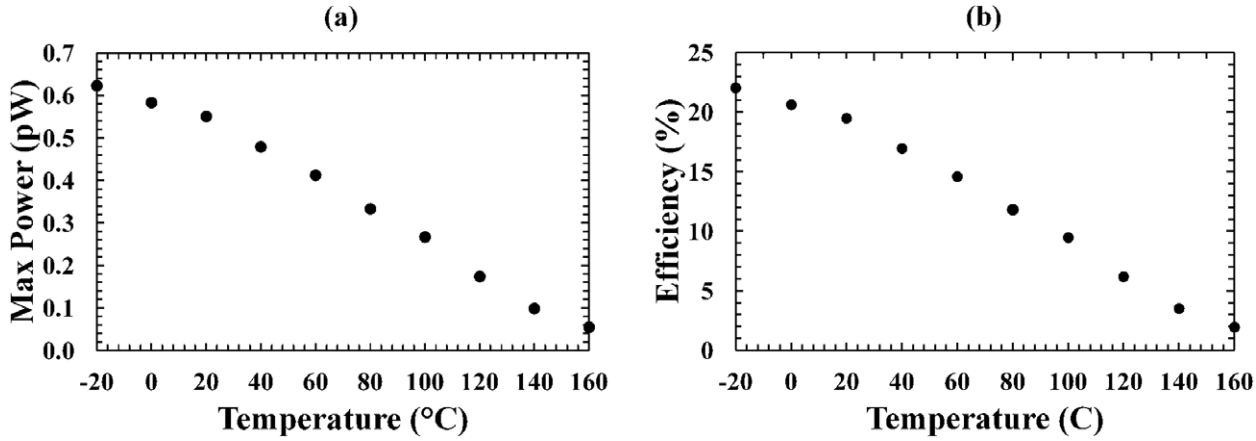

Figure 9. (a) Experimental maximum power as a function of temperature for D1. (b) Conversion efficiency (η) as a function of temperature for D1.

for D2. V_{OC} as high as 0.97 V and 0.96 V were observed for D1 and D2, respectively, at −20 °C. These values are much higher than has been previously reported (0.3 V) using a GaAs ^{55}Fe radioisotope microbattery at the same temperature [13]. This is due to the higher bandgap of $Al_{0.52}In_{0.48}P$ with respect to GaAs (at room temperature, the bandgap of $Al_{0.52}In_{0.48}P$ and GaAs are ~2.3 eV [19] and ~1.42 eV [6], respectively).

The experimental values of the short circuit current (I_{SC}) were obtained as the interception point of the curves in figure 5 on vertical axis. Figure 7 shows the I_{SC} as a function of temperature for D1, similar results were found for D2.

An unclearly defined relationship was observed for the short circuit current with temperature in the $Al_{0.52}In_{0.48}P$ ^{55}Fe radioisotope microbattery, this was due to the relatively high uncertainty of the picoammeter in measuring low currents through the photodiodes positioned in the climatic cabinet system.

The output power from each $Al_{0.52}In_{0.48}P$ photodiodes was computed by multiplying the applied bias with the correspondent current measured through the device. When the bias was increased, the output power increased to a maximum, P_m, and then decreased. Figure 8 shows the output power from D1, similar results were obtained for D2.

The magnitude of the measured maximum output power as a function of temperature is reported in figure 9(a). The magnitude of the measured maximum output power as a function of temperature is reported in figure 9(a). The conversion efficiency (η) was computed by dividing the maximum output power measured at each temperature by the maximum power (P_{th}) obtainable from the x-ray photons usefully absorbed by the device if the device conversion efficiency was 100%. P_{th} was estimated knowing the activity of the source, the emission probabilities of Mn $K\alpha$ and Mn $K\beta$ x-rays from ^{55}Fe (0.245 and 0.0338, respectively [25]), the thickness of the radioisotope x-ray source's Be window (0.25 mm), the areas of the ^{55}Fe radioactive source and $Al_{0.52}In_{0.48}P$ mesa device, the $Al_{0.52}In_{0.48}P$ device QE (calculated in section 2) and assuming an electron–hole pair creation energy of 5.8 eV (2.5 times the bandgap). P_{th} was found to be 2.8 pW. Figure 9(b) shows the efficiency as a function of temperature for D1. A conversion efficiency as high as 22% was observed at −20 °C for D1, similar results were found for D2 20%.

Table 2. Maximum output powers from the studied $Al_{0.52}In_{0.48}P$ photodiodes at particular temperatures.

Temperature (°C)	Maximum power D1 (pW)	Maximum power D2 (pW)
−20	0.62	0.60
20	0.55	0.52
80	0.33	0.35
160	0.05	0.06

At increased temperature, the magnitude of the maximum output power decreased because of its dependent on the open circuit voltage [6]. A maximimum output power as high as 0.62 pW, corresponding to 0.3 μW/Ci, was observed from the best $Al_{0.52}In_{0.48}P$ detector at −20 °C. This value is lower than the maximum output power observed by Butera *et al* [13] using a GaAs ^{55}Fe radioisotope microbattery, at the same temperature. This is mainly due to the smaller number of useful photons per second absorbed in the $Al_{0.52}In_{0.48}P$ detector (0.02×10^6 s^{-1}) with respect to the GaAs device (0.05×10^6 s^{-1}): the i-layer thickness of the $Al_{0.52}In_{0.48}P$ photodiode was 2 μm, whilst the i-layer thickness of the GaAs device was 10 μm. An advantage of the reported $Al_{0.52}In_{0.48}P$ ^{55}Fe radioisotope microbattery is that the output powers of the two 400 μm diameter $Al_{0.52}In_{0.48}P$ devices can be combined, resulting in a total microbattery output power of 1.2 pW achieved at −20 °C. Table 2 reports the maximum output powers at some significant temperatures, for both the $Al_{0.52}In_{0.48}P$ detectors studied.

The microbattery's maximum output power may be improved in the next prototype generation increasing the i-layer thickness of the $Al_{0.52}In_{0.48}P$ photodetectors so that more photons are absorbed. A better microbattery system design could be also advantageous: in the reported design, only 0.3% of the emitted photons impinged on the surface of the $Al_{0.52}In_{0.48}P$ devices and only 0.05% were actually absorbed in the devices. The number of photons per second emitted in any direction by the source was estimated knowing the activity of the source and the emission probabilities of Mn $K\alpha$ and Mn $K\beta$ x-rays

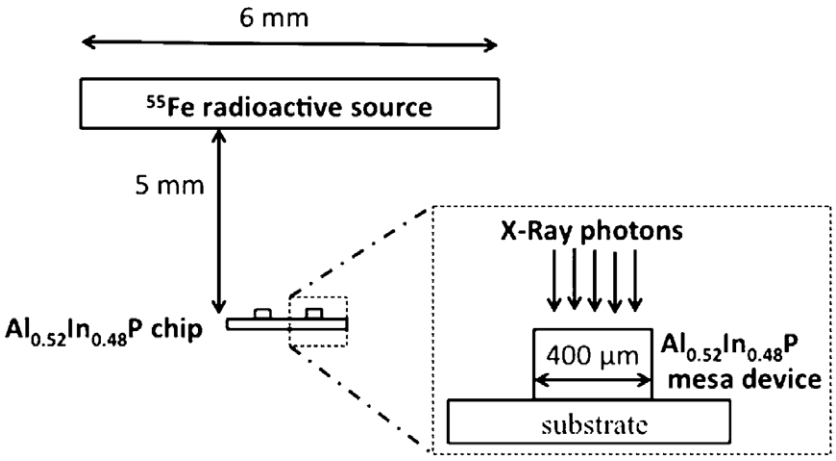

Figure 10. Schematic geometry of the $Al_{0.52}In_{0.48}P$ ^{55}Fe radioisotope microbattery system.

from ^{55}Fe (0.245 and 0.0338, respectively [25]); it was found that 6.6×10^7 photons s^{-1} are emitted by the ^{55}Fe radioactive source. Of these 6.6×10^7 photons s^{-1}, only half are emitted in the direction of the devices (we assumed that half of the photons were lost because emitted up). The number of photons per second on the devices (1.7×10^5 s^{-1}) was estimated knowing the number of photons per second emitted by the source towards the devices (3.3×10^7 s^{-1}), the thickness of the radioisotope x-ray source's Be window (0.25 mm) and the geometry of the source and detectors. Figure 10 shows schematically the geometry of the source and detector; the ratio between the area of the devices (0.25 mm^2) and the area of the radioactive ^{55}Fe source (28.27 mm^2) was calculated to be 0.0089. The number of photons on the detector was estimated by multiplying 0.0089 for the number of photons per seconds transmitted trough the x-ray source's Be window (1.9×10^7 s^{-1}). The number of photons per seconds absorbed in the devices was calculated using the Beer–Lambert law and assuming complete (100%) charge collection in the active p- and i-layers: the number of photons per second on the devices was multiplied for the device QE (calculated according equation (1)) so that 3.4×10^4 photons s^{-1} were found to be absorbed in the devices.

4. Conclusion

In this paper for the first time an $Al_{0.52}In_{0.48}P$ ^{55}Fe radioisotope microbattery is reported: a 238 MBq ^{55}Fe radioisotope x-ray source was coupled to p^+-i-n^+ $Al_{0.52}In_{0.48}P$ mesa photodiodes to achieve the conversion of nuclear energy into electrical energy. $Al_{0.52}In_{0.48}$ P is lattice matched with GaAs and is commonly used in semiconductor optoelectronics. The crystalline quality of the lattice matched $Al_{0.52}In_{0.48}P$ can be very high in comparison to III–V nitrides, IV and II–VI compounds of a similar bandgap. The doping in $Al_{0.52}In_{0.48}P$ is also easier to control than in some II–VI semiconductors. These characteristics could provide benefits in the development of microbatteries in many applications. The reported $Al_{0.52}In_{0.48}P$ ^{55}Fe radioisotope microbattery was characterised over the temperature range −20 °C to 160 °C. Increasing the temperature, the saturation current increased; whilst the open circuit voltage, the maximum power and the conversion efficiency decreased. An open circuit voltage as high as 0.97 V was measured in a single $Al_{0.52}In_{0.48}P$ p^+-i-n^+ mesa structure at −20 °C. A conversion efficiency of 22% was observed at −20 °C, taking into account attenuation from contacts and dead layer. The highest total microbattery maximum output power, obtained using the combined output powers from the two analysed mesa structures, was 1.2 pW at −20 °C; this value can be improved in the next prototype generation with a better system design. In the reported design, many of the photons emitted by the ^{55}Fe radioisotope x-ray source were lost: only 0.3% impinged the surface of the $Al_{0.52}In_{0.48}P$ devices and only 0.05% were actually absorbed in the devices.

Acknowledgment

This work was supported by STFC grant ST/M002772/1 (University of Sussex, A M B, PI). The authors are grateful to R J Airey and S Kumar at the EPSRC National Centre for III–V Technologies for device fabrication. G Lioliou acknowledge funding received from University of Sussex in the form of a PhD scholarship.

Authors' Data Statement: Data underlying this work are subject to commercial confidentiality. The authors regret that they cannot grant public requests for further access to any data produced during the study.

References

[1] Lee X and Wang C 2015 *Appl. Opt.* **54** 2219
[2] Birkholz M *et al* 2013 *J. Appl. Phys.* **113** 244904
[3] Park J H *et al* 2008 *Opt. Express* **16** 20249
[4] Bower K E, Barbanel Y A, Shreter Y G and Bohnert G W 2002 *Polymers, Phosporors, and Voltaics for Radioisotope Microbatteries* (Boca Raton, FL: CRC Press)
[5] Chandrashekhar M, Thomas C I, Li H, Spencer M G and Lal A 2006 *Appl. Phys. Lett.* **88** 0335061
[6] Sze S M and Ng K K 2007 *Physics of Semiconductor Devices* 3rd edn (New York: Wiley)
[7] Choyke W and Pensl G 1997 *MRS Bull.* **22** 25

[8] Lioliou G, Mazzillo M, Sciuto A and Barnett A M 2015 *Opt. Express* **23** 21657
[9] Lioliou G, Meng X, Ng J S and Barnett A M 2016 *Nucl. Instrum. Methods Phys. Res.* A **813** 1
[10] Bormashov V *et al* 2015 *Phys. Status Solidi* A **212** 2539
[11] Li X-Y, Ren Y, Chen X-J, Qiao D-Y and Yuan W-Z 2010 *J. Radioanal. Nucl. Chem.* **287** 173
[12] Wang H, Tang X-B, Liu Y-P, Xu Z-H, Liu M and Chen D 2015 *Nucl. Instrum. Methods Phys. Res.* B **359** 36
[13] Butera S, Lioliou G and Barnett A M 2016 *J. Appl. Phys.* **119** 064504
[14] Landis G A, Bailey S G, Clark E B, Myers M G, Piszczor M F and Murbach M S 2012 *38th IEEE Photovoltaic Specialists Conf., PVSC (Austin, TX, 3–8 June 2012)* p 002819
[15] Cheng Z, Chen X, San H, Feng Z and Liu B 2012 *J. Micromech. Microeng.* **22** 074011
[16] Sharma A, Melancon J M, Bailey S G and Zivanovic S R 2015 *IEEE Trans. Electron Devices* **62** 2320
[17] Eiting C J, Krishnamoorthy V, Rodgers S and George T 2006 *Appl. Phys. Lett.* **88** 064101
[18] Zhang Y G, Li C, Gu Y, Wang K, Li H, Shao X M and Fang J X 2010 *IEEE Photonics Technol. Lett.* **22** 944
[19] Cheong J S, Ong J S, Ng J S, Krysa A B and David J P R 2014 *IEEE J. Sel. Top. Quantum Electron.* **20** 142
[20] Cromer D T and Liberman D 1970 *J. Chem. Phys.* **53** 1891
[21] Jenkins R, Gould R W and Gedcke D 1995 *Quantitative X-ray Spectrometry* 2nd edn (Boca Raton, FL: CRC Press)
[22] Hubbell J H 1982 *Int. J. Appl. Radiat. Isot.* **33** 1269
[23] Keithley Instruments Inc 2011 Model 6487 picoammeter/ voltage source reference manual, 6487-901-01 Rev B Cleveland
[24] Chandrashekhar M, Duggirala R, Spencer M G and Lal A 2007 *Appl. Phys. Lett.* **91** 053511
[25] Schotzig U 2000 *Appl. Radiat. Isot.* **53** 469